EPJ Web of Conferences **274**, 01008 (2022) https://doi.org/10.1051/epjconf/202227401008
XVth Quark Confinement and the Hadron Spectrum

Light-meson scattering dispersive analyses and light-scalar meson spectroscopy. Where do we stand?

José R. Peláez[1,*]

[1]Departamento de Física Teórica and IPARCOS, Universidad Complutense, 28040 Madrid. Spain

Abstract. In this talk I reviewed the present status and recent progress on light-meson scattering analyses, by means of dispersive or analytic methods. The recent application of these model independent techniques have settled the controversy about the existence and parameters of long debated light meson resonances. I will thus discuss here the state of the art and recent changes on our knowledge about the spectroscopy of light scalar mesons when observed from such scattering processes.

1 Introduction

The scattering of two light pseudoscalar mesons is of interest by itself, but also for several other reasons. In particular, pions and kaons, being the lightest hadrons appear in the final states of almost all strongly interacting processes, and as soon as there are at least two of them, their rescattering plays a fundamental role in the whole description. Also, since pions, kaons and the eta are the pseudo Goldstone bosons of the spontaneous chiral symmetry breaking of QCD, their interactions are essential for a detailed understanding of this breaking. Moreover, they are also a relevant source of data, the main one in many cases, to determine the existence and parameters of the resonance states that constitute the hadron spectrum. However, the description of these scattering processes has been difficult and particularly controversial in the scalar sector. To illustrate this controversy I will follow the evolution and latest developments in the Review of Particle Properties (RPP). Although listed with different names for many years, it is only in its 2022 edition that the RPP [1] has removed the "Needs confirmation" label of the lightest strange resonance or $K_0^*(700)$ resonance, traditionally known as the κ meson. The existence of this meson, as well as that of the σ or $f_0(500)$ meson, settled in the 2012 edition, had been the subject of decade-long controversies. Many studies have been dedicated to understand meson-meson scattering and the resonances that appear there, but a particularly relevant role in the final recognition of these states has been played by rigorous dispersive treatments of meson-meson scattering, to which I dedicate this review talk, which I have built mostly from the recent and more detailed reviews in [2–4] as well as from the RPP [1]. In those reviews it is possible to find a more complete list of references than the one I can provide here, for which I apologize.

Once the $\kappa/K_0^*(700)$ and $\sigma/f_0(500)$ existence, mass and widths are determined, the emerging picture for the spectroscopic classification of light scalars below 1.8 GeV is shown in Fig.1. There seems to be a light scalar nonet below 1 GeV and another one above, plus an

*e-mail: jrpelaez@fis.ucm.es

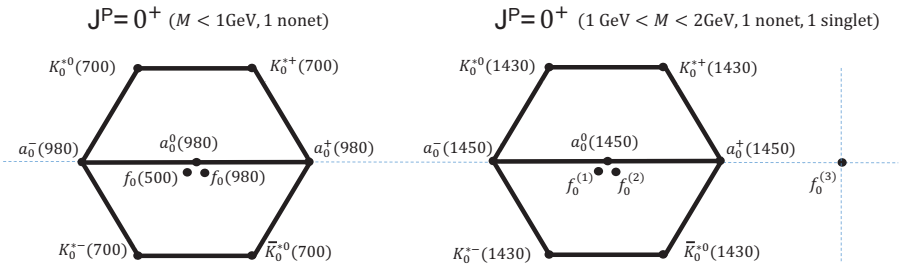

Figure 1. Spectroscopic classification of scalar mesons below 2 GeV in terms of two $SU(3)$ nonets and a singlet. We do not identify the f_0 states above 1 GeV, because their mixing pattern to form the observed $f_0(1370)$, $f_0(500)$ and $f_0(1710)$ is still under debate.

additional state. The mixing of the f_0^1, f_0^2, f_0^3 states to form the observed $f_0(1370)$, $f_0(1500)$ and $f_0(1710)$ is still under debate. The existence of an additional singlet f_0 state around 1.5 GeV outside the nonets is very consistent with the expectations for the lightest glueball. It is worth mentioning that the two nonets do not follow the expected mass hierarchy of ordinary $q\bar{q}$ mesons within the Quark Model. In particular, strange resonances within each nonet are not ∼200 MeV heavier than their non-strange counterparts. This suggests the existence of possibly large, if not dominant, tetraquark, molecular or meson-meson cloud components. Much attention has been also devoted to this topic, and there is mounting evidence from other processes supporting that these are indeed non-ordinary mesons, Unfortunately such a discussion lies beyond the scope of this talk. Suffices it to say here that a good description of meson-meson interactions and a rigorous determination of each resonance mass, width and couplings to meson-meson states are very relevant for this discussion too. Let us then focus on dispersive analysis, since they provide precise and model-independent results. First of all we describe the problems to be addressed and how dispersion relations tackle them.

2 The data and model problems in meson-meson scattering

The long debate and controversy about meson-meson scattering and light scalars was caused by several issues that we can naively group under the label of the "data problem" and the "model problem".

The data problem is due to the fact that there are no direct meson-meson scattering experiments and the data is thus extracted from other processes. There are a few very precise and accurate data points on the $\pi\pi$ scattering phase obtained from $K \to \pi\pi\ell\nu_\ell$ decays, although obviously limited to energies less than the mass of the kaon. The rest of meson-meson scattering data were extracted from the so-called one-pion-exchange contribution to meson-meson to meson-meson nucleon. This is depicted in Fig.2. Note that within this approximation, the initial meson-meson state is not well defined, since it contains a virtual pion, and of course there are additional contributions that have to be modelled like re-absorption, A_2-exchange, etc... On top of that a partial wave analysis of the whole process is needed. All these approximations lead to large systematic uncertainties. As an illustration we show in Fig.3 existing data on the scalar ($\ell = 0$) phase shifts of $\pi\pi \to \pi\pi$ and $\pi K \to \pi K$ scattering for definite $I = 0$ and $I = 1/2$ isospin, respectively. Also respectively, these are the channels where the $\sigma/f_0(500)$ and $\kappa/K_0^*(700)$ appear as resonances. Dispersion relations address this data

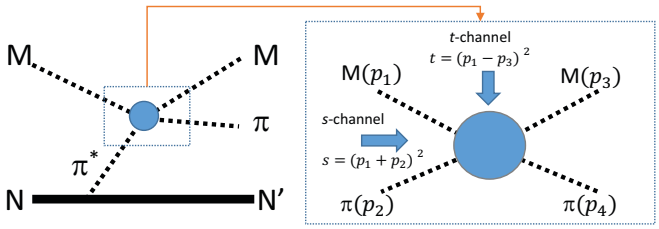

Figure 2. Schematic representation of the extraction of meson-meson scattering data, where $M = \pi, K$, by considering it a sub-process that contributes to a larger $MN \to M\pi N$ collision. For the extraction, the experiment looks for the kinematic region where the exchanged virtual pion is close to being real. In the right panel we define the Mandelstamm s and t variables, which correspond to the total energy squared in the center of mass of their respective scattering channels.

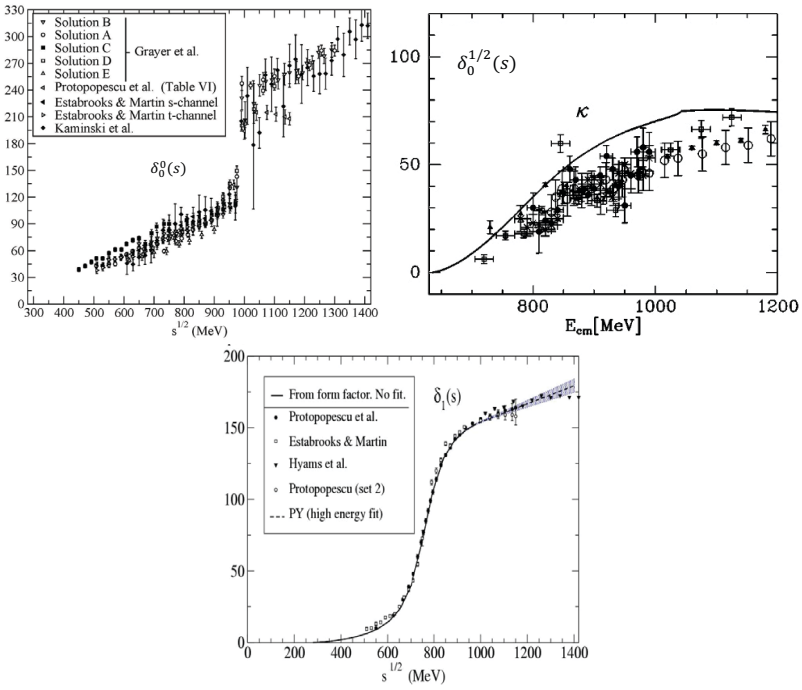

Figure 3. Data on meson-meson scattering partial-wave phase-shifts δ_ℓ^I, where I is the isospin and ℓ the angular momentum. Up-Left: $\pi\pi \to \pi\pi$ in the scalar-isoscalar channel. Up-right: $\pi K \to \pi K$ in the scalar-isospin 1/2 channel. Note in both cases the inconsistencies within different data sets, but also within the same experiment. Bottom: $\pi\pi \to \pi\pi$ in the vector-isovector channel. Figures taken from [2], [5] and [2], respectively, see references therein.

problem by providing, on the one hand, stringent tests based on first principles, to discard inconsistent data points and, on the other hand, constraints for the data fits.

The model problem has two sides. On the one hand, for many years relatively crude models were quite enough to describe the data, given their large uncertainties and inconsistencies. Very often theoretical analyses were semi-quantitative at best, and, in the case when uncer-

tainties were provided, these were mostly due to statistical errors without any systematic uncertainty estimate. Even worse, different analyses could use different sets of incompatible data.

On the other hand, scalar resonances are frequently very or extremely wide, as in the $\sigma/f_0(500)$ and $\kappa/K_0^*(700)$ cases, whose widths are comparable to their masses. Moreover, they frequently overlap among themselves or with kinematic singularities like the $K\bar{K}$ threshold, as in the $f_0(980)$ and $a_0(980)$ case, or with other dynamical features like the Adler zeros required by the spontaneous chiral symmetry breaking pattern of QCD. As a consequence, many of them do not exhibit clear "peaks" in the modulus of the scattering amplitude or their corresponding rapid $\sim 180^o$ phase movement in the amplitude phase. Thus, they are not easily identifiable from the data. Examples of nice rapid phase growth can be found in the right panel of Fig.3 around 770 MeV that corresponds to the $\rho(770)$ vector resonance, but also in the left panel around 1000 MeV, corresponding to the $f_0(980)$. However, no such rapid phase motion is seen in the same panel around 500 MeV (the nominal mass of the $\sigma/f_0(500)$) nor in the central panel around 700 MeV (the nominal mass of the $\kappa/K_0^*(700)$). For these reasons, the naive identification of resonances with peaks in the amplitude is no longer valid. Nor is valid the familiar Breit-Wigner formalism, which is devised for narrow resonances, well isolated from other analytic features. For all these reasons, resonances should be rigorously identified from their associated poles in the second Riemann sheet of the complex s-plane. Customarily, their masses and widths are then defined from their pole position as $\sqrt{s_{pole}} = M - i\Gamma/2$.

However, the continuation to the complex plane from the segment of the real axis where data is available is a delicate mathematical problem. Determining poles from simple models that do not implement the correct analytic structure and dynamical features can lead to spurious determinations. In Fig.4 we show the analytic structure in the s-complex plane of the $\pi\pi \to \pi\pi$ (top) and $\pi K \to \pi K$ partial waves (bottom). The opening of physical channels above their threshold energies gives rise to a right cut in the real axis extending from threshold to infinity. Actually, this cut is made of a superposition of cuts, one for each open channel. Crossing symmetry implies that the corresponding cuts of crossed channels are also seen as a left cut in the channel under consideration, extending from $-\infty$ to $(m_1 - m_2)^2$, where m_1 and m_2 are the masses of the two initial mesons. In addition, there is a circular cut, due to the partial wave projection, of radius $|s| = m_1^2 - m_2^2$. In that figure we see that in the case of the rho (and the vector $K^*(890)$), their poles sit very close to the real axis and far from any other analytic features. It is for this reason that it is seen as a nice peak in the data with an associated rapid phase motion. The $f_0(980)$ pole is also very close to its nominal value, and that is why its phase motion is easily seen in the data, although it does not quite reach a 180^o change and when seen up close is somewhat distorted by the presence of the nearby $K\bar{K}$ threshold. In contrast, both the $\sigma/f_0(500)$ and $\kappa/K_0^*(700)$ are not only very deep in the complex plane, so that their associated peak would be much wider and much less prominent, but they are as close to the real axis at their nominal mass as to the first threshold in their channel or to the left or circular cuts. Moreover, they are also relatively close to the Adler zeros in their partial waves. Their extreme wideness and the presence of near additional analytic and dynamical structures hide their resonance shape in the real axis. It is therefore very important to have a good description of the amplitude in the real axis, consistent with the analyticity constraints. As we will see next, dispersion relations also address this model problem by providing the analytic continuation to the complex plane required for a rigorous determination of the existence of poles and a precise determination of their parameters.

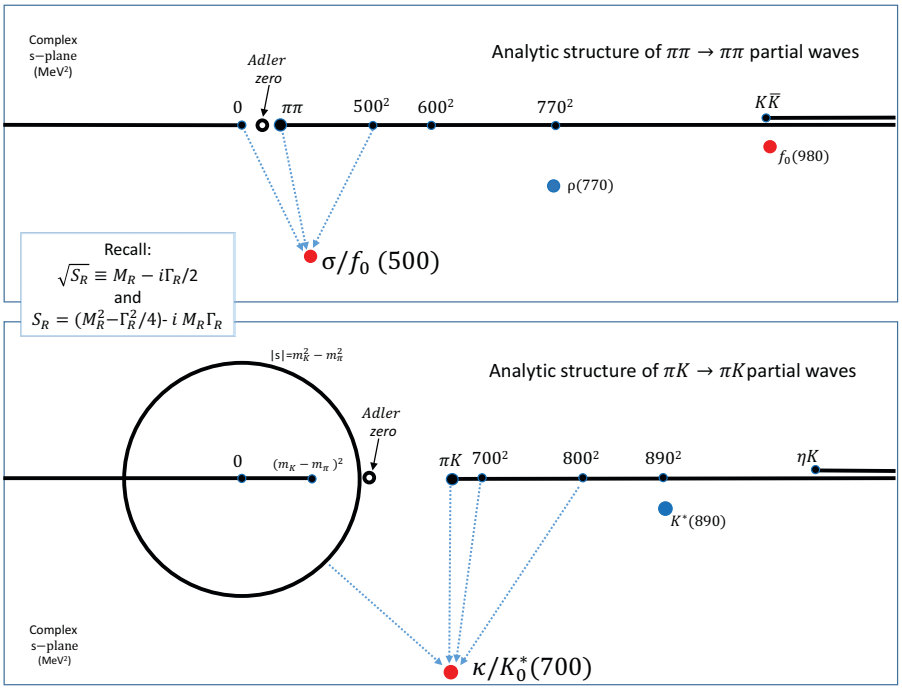

Figure 4. Analytic structure in the s-complex plane of the $\pi\pi$ (top) and $\pi K \to \pi K$ partial waves (bottom). Figure taken from [4].

3 Dispersion Relations

These are nothing but applying Cauchy's Integral Formula, which yields the value of an analytic function inside a given contour C as an integral of the function over the contour, i.e.:

$$t(s) = \frac{1}{2\pi i} \oint_C ds' \frac{f(s')}{s' - s}.$$

Given the generic analytic structure discussed in Fig.4, we apply Cauchy's Theorem above, along a typical contour as that shown in Fig.5, leading to an equation of the form:

$$t(s) = \int_{s_{th}}^{\infty} \frac{Imt(s')}{s - s'} ds' + LC + CC, \tag{1}$$

where LC and CC stand for similar integrals for the left and, if present, circular cuts. In case the amplitude $t(s)$ does not tend to infinity sufficiently fast to make the contribution from the large circular part of the contour vanish as its radius tends to infinity, we have to "subtract it". This means that we divide the integrand by a polynomial and then the amplitude will be constrained by the dispersion relation up to such a polynomial, whose coefficients are called subtraction constants.

Note that to apply Cauchy's Theorem we need a one-variable amplitude, whereas meson-meson scattering amplitudes depend on both s and t. Two different ways to proceed then lead to the two most popular kinds of dispersion relations:

1) **Fixed-variable dispersion relations.** The most common ones are the fixed-t dispersion relations. Their analytic structure is simpler because they do not have a circular cut and

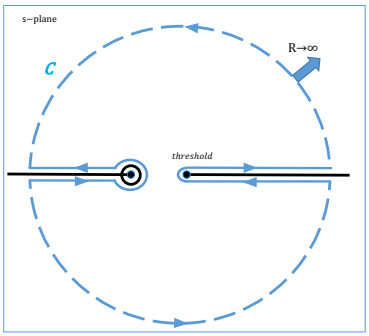

Figure 5. Typical contour of integration to apply Cauchy's Theorem and obtain a Dispersion Relation. The curved part of the contour is taken to ∞ and vanishes if the integrand tends to zero sufficiently fast, leaving only the integrals surrounding the cuts. Since amplitudes in the lower plane are the conjugate of their values in the upper one, the integrands can be rewritten in terms of imaginary parts of the amplitudes only, leading to Eq.(1). Figure taken from [4]

the left cut extends from ∞ to $s = -t$. Among these, the most popular ones are the Forward Dispersion Relations (FDRs), because the left-cut contribution is easily rewritten in terms of the physical region, giving very simple expressions. Remarkably, the algebraic manipulations for this do not limit their applicability region. In practice, they have been implemented up to 1.42 GeV for $\pi\pi \to \pi\pi$ [6] and 1.47 GeV for $\pi K \to \pi K$ [3]. Finally, the imaginary part of the forward amplitude is directly related through the Optical Theorem to the total meson-meson scattering cross section, for which direct data are available. However, they are less used to determine poles because they need additional continuation methods to the adjacent Riemann sheet and because they mix different angular momenta, since they do not constraint each partial waves, but the full amplitude. With the appropriate choice of isospin basis they can be made very precise due to the positivity of their integrands.

2) **Partial-wave dispersion relations and Roy-like Equations**

Once again, the complicated parts are the contributions from left and circular cuts. Here there are again two generic approaches.

The first one leads to the so-called "Unitarization Methods". Here one writes the dispersion relation not for the partial wave, but for its inverse. This is because in the elastic case, unitarity fixes completely its imaginary part over the right cut, which can be integrated exactly. The rest of the amplitude, including subtraction terms and left or circular cut contributions are then approximated, often up to a given order of an effective Lagrangian. This can give rise to relatively simple analytic expressions and a connection to QCD parameters. They can even be generalized to the cases with several two-body coupled channels. They have become very popular, but do not aim at precision and lie beyond our present scope, so that we refer the reader to the reviews [2, 4] and references therein.

The second one aims at a rigorous implementation of the left and circular cuts by using crossing symmetry to rewrite them in terms of partial waves in the physical region. For $\pi\pi$ scattering with two subtractions they are called Roy equations [7], and with one subtraction are GKPY equations [8]. Generically we will refer to them as Roy-like equations. For equal input, the former are more precise at threshold and the latter in the resonance region. For $\pi K \to \pi K$ they are called Roy-Steiner equations, originally derived for πN scattering [9, 10]. The advantage is that they are formulated directly in terms of partial waves, and provide constraints for each one of them. However, this implies that when re-expressing the left cut, the partial waves of the crossed channel become coupled with those of the direct channel. This gives rise to an infinite set of coupled dispersion relations. In practice, only the lowest waves (S, P or even D) are implemented dispersively and higher waves are taken as input. The other relevant caveat is that in their common form they are only applicable

up to energies around 1.1 GeV. Less relevant is that, contrary to FDRs, they also need the t dependence at high energies, which is much worse known from data than that for $t = 0$.

At this point, there are two general strategies to use dispersion relations:

A) **Solve the equations in some region.** Typically the S and P waves for $\pi\pi \to \pi\pi$ or $\pi K \to \pi K$ are solved below some energy below 1 GeV, where the solution is known to be unique, and the higher energies and other waves are input. Additional constraints for Chiral Perturbation theory may also be imposed in some cases, which decreases the uncertainty due to the data input only. See [11–15].

B) **Use the relations as checks of data or constraints on fits (Data driven approach)** The first use is to discard data sets or points that are very inconsistent with dispersion relations, particularly in the very conflicting S-wave. Next one obtains "Unconstrained Fits" to the "not too inconsistent" data (UFD), in all regions and for all partial waves. Then these UFD parameterizations are used as a starting point of new "Constrained Fits to Data" (CFD) imposing the dispersive constraints as penalty functions in the fit. This results in constrained fits for all partial waves satisfying dispersion relations within the data uncertainties in a relatively uniform way for all waves and energies of interest. This method also allows to impose as constraints Roy-like equations simultaneously with different number of subtractions, limited to roughly 1.1 GeV, but also FDRs up to 1.42 GeV for $\pi\pi$ and 1.6 GeV for $\pi K \to \pi K$, as well as the Roy-Steiner constraints for $\pi K \to \pi K$ and $\pi\pi \to K\bar{K}$ simultaneously. This is the approach followed by our group in a series of works dealing with those three processes [2–4, 6, 8, 16–18].

4 Results

In Fig.6 we illustrate the "data driven" procedure. In column one, we show how the UFD do not satisfy well the three independent FDRs, particularly in the areas marked with red ellipses. However, in the next column we see that all FDRs are well satisfied. Similarly with columns three and four, but for the three GKPY equations for the lowest partial waves. A similar situation is shown in Fig.7, now for the scalar wave of isospin 1/2 for $\pi K \to \pi K$, where the $\kappa/K_0^*(700)$ appears. Actually, we see that *using the same UFD input in the physical region* of that wave, the output of three different Roy-like equations obtained from different formalisms disagree. The $\kappa/K_0^*(700)$ pole obtained from each one of them would be different and inconsistent from one another by several tens of MeVs. This is fixed with the constrained fits. However, in the physical region the CFD and UFD fits look very consistent. It is the change in the region below $K\bar{K}$ threshold in the crossed $\pi\pi \to K\bar{K}$ channel that makes the difference. This is a strong warning against the use of simple models just fitted to data in the physical region, and then looking for poles without checking the fulfillment of the dispersive representation.

One might of course wonder if, by imposing the dispersive constraints, the data is no longer described. This is not the case. The CFD seem to deviate a little form certain data points, but the description is still acceptable. This is illustrated in the left panel of Fig.8, where the UFD and CFD of the $\pi\pi$ in the scalar-isoscalar wave are barely distinguishable except around 1 GeV in the $f_0(980)$ region. Somewhat larger deviations from the UFD can be found in higher waves or higher energies were the data are scarce or inconsistent. A similar situation occurs for $\pi K \to \pi K$ and $\pi\pi \to K\bar{K}$ scattering, although in the latter case, the CFD differs largely from the UFD in the unphysical region, below $K\bar{K}$, where data cannot exist. However, this region is relevant for the unphysical cut contributions to $\pi K \to \pi K$ Roy-Steiner equations and to determine the $\kappa/K_0^*(700)$ pole existence and parameters.

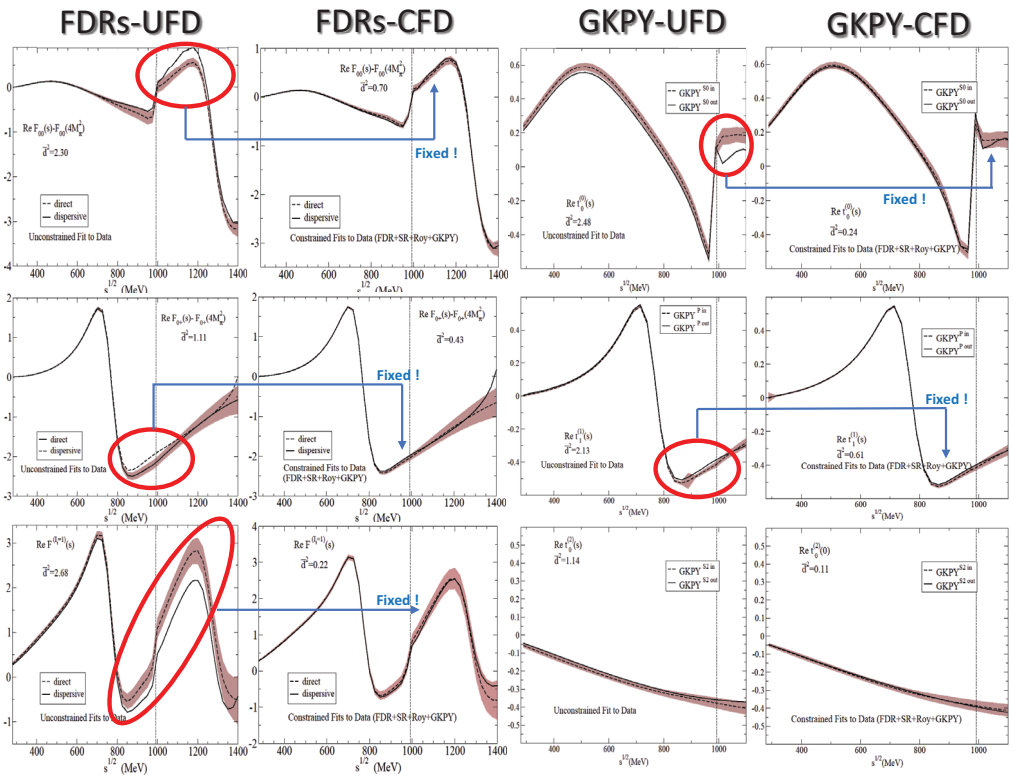

Figure 6. Unconstrained fits to data (UFD) do not satisfy well dispersion relations, as seen in column one for FDRs and column 3 for GKPY equations, particularly in the regions highlighted by red ellipses. This is fixed by the Constrained fits to data CFD in columns two (FDRs) and four (GKPY).

In Fig.9 we show how the "Solve" approach and the "Data driven" approach described above are fairly consistent, which is a nice check of the robustness of the approach, given their different inputs and implementation methods.

Finally, once a description of partial-wave data consistent with the dispersive representation has been achieved, one can use the very same dispersion relations to obtain a mathematically rigorous and model-independent determination of the poles. For this one has first to make sure that they converge in the region of the complex plane that includes those resonances. This was done for $\pi\pi$ in [14] and for $\pi K \to \pi K$ in [15]. See [3] for a comprehensive description and extension of these analyses. Fortunately both the controversial $\sigma/f_0(500)$ and $\kappa/K_0^*(700)$ fall inside the domain of applicability of some Roy-like dispersion relations. Note that, for all means and purposes they appear in the elastic region of $\pi\pi \to \pi\pi$ and $\pi K \to \pi K$ scattering, respectively. In that region, the S-matrix in the second sheet, were poles live, is nothing but the inverse of the S-matrix in the first sheet, which is directly given by the dispersion relations.

Thus, in tables 1 and 2 we show the pole determinations from Roy-like dispersive analyses for the $\sigma/f_0(500)$ and $\kappa/K_0^*(700)$ resonances. We can see that the agreement is remarkable and the precision is at the level of the 10-20 MeV, being conservative. These determinations are responsible for the removal of their "Needs Confirmation" labels in the RPP, which the $\kappa/K_0^*(700)$ held as late as 2021.

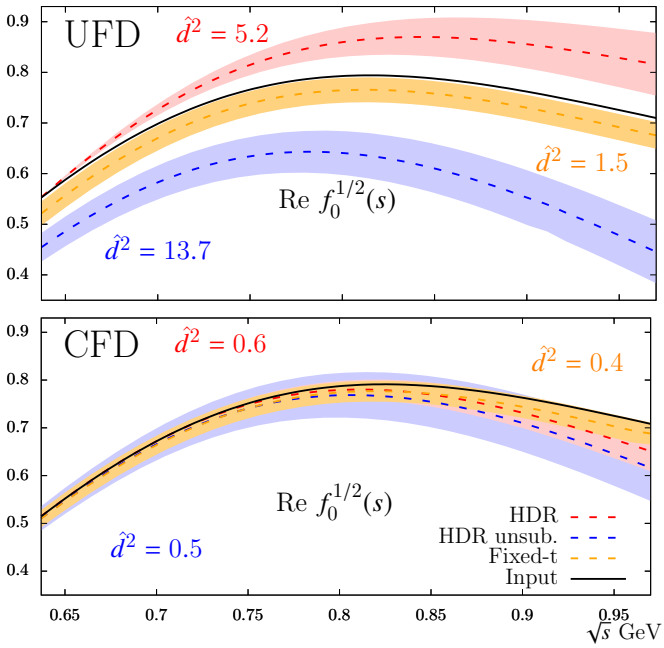

Figure 7. Top: We show how the outputs of three different Roy-like dispersion relations, obtained from hyperbolic dispersion relations with one subtraction (HDR) or unsubtracted (HDR unsub.) or from fixed-t dispersion relations, are inconsistent for the $\pi K \to \pi K$ scalar-isospin 1/2 partial wave, when using *the same* Unconstrained Fits to Data (UFD) as input in the integrals. Bottom: Good agreement within uncertainties is obtained from Constrained Data Fits (CFD), which do not change much the physical description of data but the unphysical region of the crossed $\pi\pi \to K\bar{K}$ channel. Figures taken from [17].

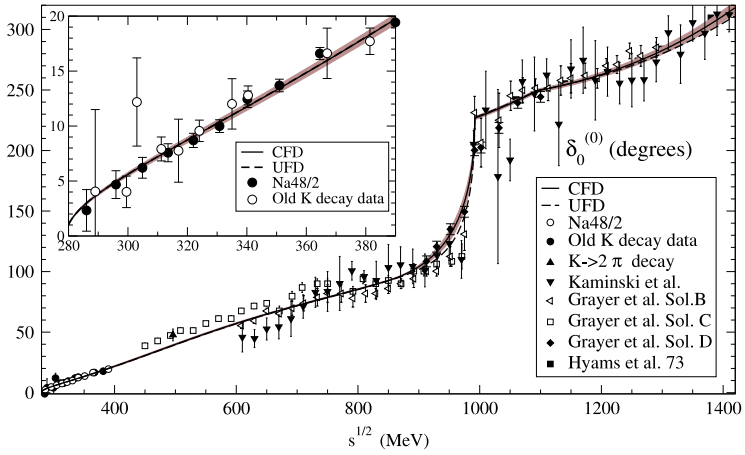

Figure 8. The $\pi\pi$ scalar isoscalar phase shift is well described both with the Unconstrained Fits to Data (UFD) or dispersively Constrained Fits to Data (CFD). Figure taken from [2].

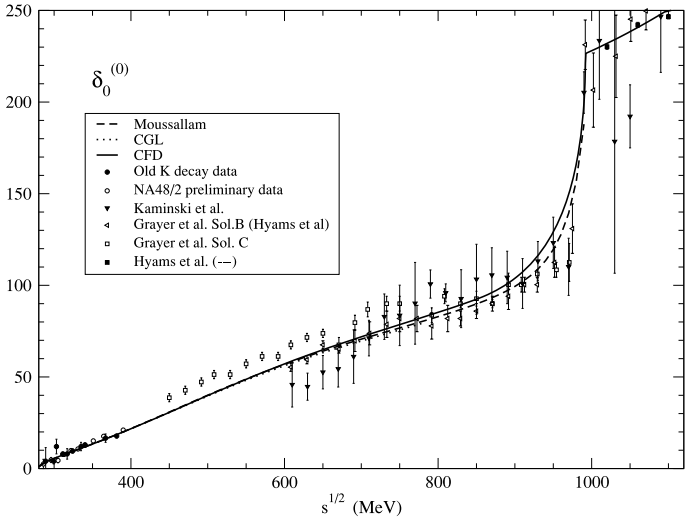

Figure 9. We show the central values of Roy-like analysis following the "Solve" ("CGL" stands for [12] and "Moussallam" for [19]) versus the "Data driven" [8] approaches described in the text. They are fairly consistent, particularly since we have not plotted their associated uncertainty bands to make all curves visible. Figure taken from [2].

Table 1. $\sigma/f_0(500)$ pole determinations using Roy or GKPY equations and the conservative dispersive estimate [2] which covers them. For the latter we have corrected a typo in the error of Im $\sqrt{s_{pole}}$ which read ±12 MeV instead of ±15 MeV.

$\sigma/f_0(500)$	$\sqrt{s_{pole}}$ (MeV)	$\lvert g\rvert$ (GeV)
Refs. [14, 20]	$(441^{+16}_{-8}) - i(272^{+9}_{-12.5})$	$3.31^{+0.35}_{-0.15}$
Ref. [19]	$(442^{+5}_{-8}) - i(274^{+6}_{-5})$	-
Ref. [6]	$(457^{+14}_{-13}) - i(279^{+11}_{-7})$	$3.59^{+0.11}_{-0.13}$
Conservative Dispersive Estimate		
Ref. [2]	$(449^{+22}_{-16}) - i(275 \pm 15)$	$3.45^{+0.25}_{-0.29}$

Table 2. $\kappa/K_0^*(700)$ dispersive pole determinations using Roy-Steiner equations.

$\kappa/K_0^*(700)$	$\sqrt{s_{pole}}$ (MeV)	$\lvert g\rvert$ (GeV)
Ref. [15]	$(658 \pm 13) - i(279 \pm 12)$	
Ref. [3]	$(648 \pm 7) - i(280 \pm 16)$	3.81 ± 0.09

5 Summary

In this talk I have briefly reviewed the use of rigorous dispersive precision approaches to obtain descriptions of $\pi\pi \to \pi\pi$, $\pi K \to \pi K$ and $\pi\pi \to K\bar{K}$ data, that are simultaneously consistent with dispersion relations. These are constraints imposed from first principles like causality, crossing, etc.. that also provide a rigorous continuation to the complex plane. This has allowed to settle the longstanding controversy about the existence of the lightest

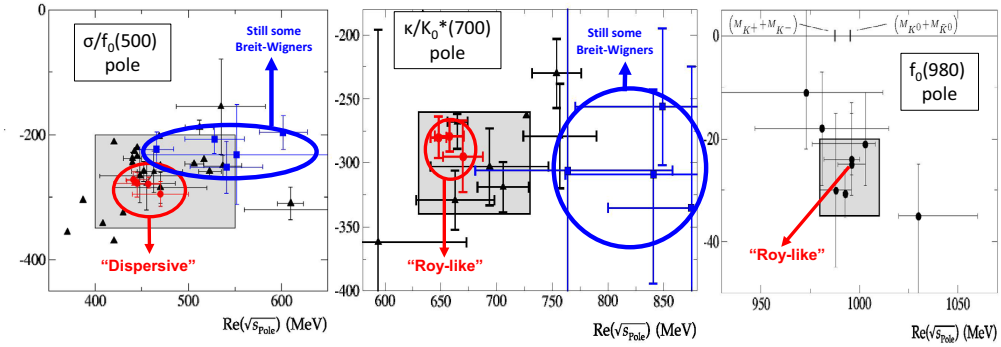

Figure 10. Present situation of T-matrix poles of light scalars in the RPP [1]. The grey areas cover the RPP estimates for each resonance pole mass and width, where $\sqrt{s_{pole}} = M - i\Gamma/2$. We have highlighted in red the "Roy-like" dispersive determinations. Note that poles for traditional Breit-Wigner parameterizations, highlighted in blue, are also listed since they are still widely used, although they are not appropriate for these poles. Left: for the $\sigma/f_0(500)$ meson. Center: for the strange $\kappa/K_0^*(700)$ resonance. Right: For the $f_0(980)$, which has never been too controversial, but can also be determined dispersively. Original figures taken from [1]. The highlighting and commenting of red and blue areas is ours.

and widest scalar resonances: the $\sigma/f_0(500)$ and $\kappa/K_0^*(700)$. We summarize their present situation in Fig.10 and tables 1 and 2.

With the confirmation of these two states from meson-meson dispersive analyses, our present understanding of light scalar mesons is that of Fig.1. Two nonets and one singlet exist below 2 GeV. One nonet lies below 1 GeV and another one above. Their inner mass hierarchies, particularly for the lowest one, are at odds with the expectations for ordinary quark-antiquark mesons. The fine details of their nature and possible mixing schemes are still the subject of present study.

Acknowledgments

I would like to thank the organizers for their kind invitation and the excellent organization and stimulating atmosphere of the conference. Work partially funded by the Spanish MINECO grant FPA2016-75654-C2-2-P and the European Union's Horizon 2020 research and innovation programme under grant agreement No 824093 (STRONG2020).

References

[1] R.L. Workman et al. (Particle Data Group), PTEP **2022**, 083C01 (2022)
[2] J.R. Pelaez, Phys. Rept. **658**, 1 (2016), 1510.00653
[3] J.R. Peláez, A. Rodas, Phys. Rept. **969**, 1 (2022), 2010.11222
[4] J.R. Peláez, A. Rodas, J.R. de Elvira, Eur. Phys. J. ST **230**, 1539 (2021), 2101.06506
[5] J.A. Oller, E. Oset, J.R. Pelaez, Phys. Rev. D **59**, 074001 (1999), [Erratum: Phys.Rev.D 60, 099906 (1999), Erratum: Phys.Rev.D 75, 099903 (2007)], hep-ph/9804209
[6] R. García-Martín, R. Kaminski, J.R. Peláez, J. Ruiz de Elvira, Phys.Rev.Lett. **107**, 072001 (2011), 1107.1635
[7] S.M. Roy, Phys.Lett. **36B**, 353 (1971)
[8] R. Garcia-Martin, R. Kaminski, J.R. Pelaez, J. Ruiz de Elvira, F.J. Yndurain, Phys. Rev. D **83**, 074004 (2011), 1102.2183

[9] J. Baacke, F. Steiner, Fortsch. Phys. **18**, 67 (1970)
[10] F. Steiner, Fortsch. Phys. **19**, 115 (1971)
[11] B. Ananthanarayan, G. Colangelo, J. Gasser, H. Leutwyler, Phys. Rept. **353**, 207 (2001), hep-ph/0005297
[12] G. Colangelo, J. Gasser, H. Leutwyler, Nucl. Phys. B **603**, 125 (2001), hep-ph/0103088
[13] P. Buettiker, S. Descotes-Genon, B. Moussallam, Eur. Phys. J. C **33**, 409 (2004), hep-ph/0310283
[14] I. Caprini, G. Colangelo, H. Leutwyler, Phys.Rev.Lett. **96**, 132001 (2006), hep-ph/0512364
[15] S. Descotes-Genon, B. Moussallam, Eur. Phys. J. **C48**, 553 (2006), hep-ph/0607133
[16] J.R. Pelaez, A. Rodas, Phys. Rev. D **93**, 074025 (2016), 1602.08404
[17] J.R. Peláez, A. Rodas, Phys. Rev. Lett. **124**, 172001 (2020), 2001.08153
[18] J.R. Pelaez, A. Rodas, Eur. Phys. J. C **78**, 897 (2018), 1807.04543
[19] B. Moussallam, Eur. Phys. J. **C71**, 1814 (2011), 1110.6074
[20] H. Leutwyler, AIP Conf. Proc. **1030**, 46 (2008), 0804.3182